Available online at www.sciencedirect.com

SCIENCE DIRECT®

Tectonophysics 391 (2004) 315–324

TECTONOPHYSICS

www.elsevier.com/locate/tecto

The rupture process during the 1999 Düzce, Turkey, earthquake from joint inversion of teleseismic and strong-motion data

Nur Umutlu[a,*], Kazuki Koketsu[b], Claus Milkereit[c]

[a]*Earthquake Research Department, General Directorate of Disaster Affairs, Ministry of Public Works and Settlement, Eskişehir Yolu, Lodumlu, Ankara 06530, Turkey*

[b]*Earthquake Research Institute, University of Tokyo, Bunkyo-ku, Tokyo 113-0032, Japan*

[c]*GeoForschungsZentrum Potsdam, Telegrafenberg, Potsdam 14473, Germany*

Accepted 3 June 2004
Available online 8 September 2004

Abstract

Teleseismic and strong-motion data are inverted to determine the rupture process during the November 1999 Düzce earthquake in NW Turkey. The fault geometry, rise time and rupture velocity are determined from the aftershock distribution and preliminary inversions of the teleseismic data. Joint inversion of the teleseismic and strong-motion data is then carried out for the slip distribution. We obtain the strike 264°, dip 64°, rake −172°, seismic moment 5.0×10^{19} N m (M_w 7.1), and average stress drop 7 MPa. This earthquake was characterized by bilateral fault rupture and asymmetric slip distribution. Two asperities (areas of large slip) are identified, the eastern one being 1.5 times larger than the western one. The derived slip distribution is consistent with the aftershock distribution, surface rupture and damage. The point of rupture initiation in this Düzce earthquake coincided with the eastern tip of the aftershock distribution of the August 1999 Izmit earthquake.

Keywords: Düzce earthquake; Teleseismic waveforms; Strong-motion waveforms; Rupture process; Joint inversion; Asperity

1. Introduction

The Düzce earthquake (moment magnitude, M_w, 7.1; determined by the U.S. Geological Survey) struck northwestern Turkey, on the western part of the North Anatolian Fault (NAF) system (Fig. 1), on November 12, 1999, about 3 months after the August 17, 1999 Izmit earthquake, causing more than 800 fatalities. The Sapanca-Bolu (SABO) seismograph network, which is jointly operated by GeoForschungsZentrum Potsdam (GFZ) and the Earthquake Research Department of Turkey (ERD), determined its epicenter as 40.82°N, 31.20°E and its focal depth to be 12.5 km (Milkereit et al., 2000).

This earthquake was expected, since its source area was the only segment of the western NAF that had not ruptured during the seismic sequence from the 1939 Erzincan earthquake to the 1999 Izmit event (Akyüz

* Corresponding author. Danish Lithosphere Center, Øster Voldgade 10, 1350 Copenhagen K, Denmark.
E-mail address: nu@dlc.ku.dk (N. Umutlu).

0040-1951/$ - see front matter © 2004 Elsevier B.V. All rights reserved.
doi:10.1016/j.tecto.2004.07.019

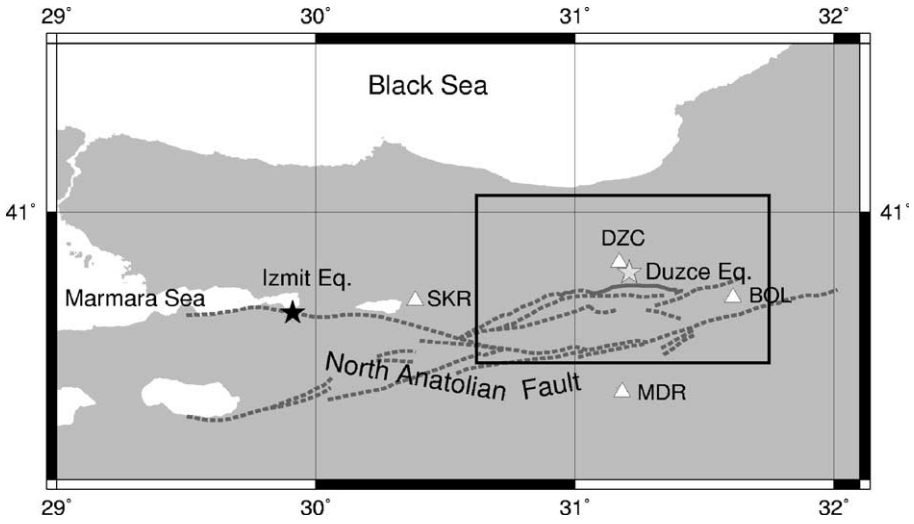

Fig. 1. Index map of the study region. Star symbols indicate the epicenters of the Düzce (gray) and Izmit (black) earthquakes. The western part of the North Anatolian Fault system is shown with thick dashed lines in gray. The triangles with three-letter codes denote the four strong motion stations closest to the epicenter of the Düzce earthquake, which provided data for our waveform inversion. The rectangle encloses the region illustrated in Fig. 2.

et al., 2002). According to Parsons et al. (2000), the latter earthquake brought the crust in the epicentral area of the Düzce earthquake closer to the condition for shear failure. Iio et al. (2002) suggested that aftershocks of the Izmit earthquake indicated afterslip, which could significantly concentrate stress in the epicentral area of the Düzce event. In order to investigate these views, it is necessary to compare the aftershock distribution with the slip distribution from analysis of the rupture process of the Düzce earthquake.

Tibi et al. (2001) previously studied this rupture process applying the multiple point source analysis method of Nábêlek (1984), using teleseismic seismograms provided by the Data Management Center of the Incorporated Research Institutions for Seismology (IRIS-DMC). They determined the focal mechanism of the Düzce earthquake to be right-lateral with strike, dip and rake angles of 263°, 62° and −176°, respectively. The rupture propagated bilaterally over a 55×20-km fault plane, with a velocity of about 2 km/s. Kiratzi and Louvari (2001) obtained a similar result. Ayhan et al. (2001) have also estimated the fault geometry and slip distribution of this coseismic rupture using GPS data. In addition to the teleseismic waveforms, strong-motion waveforms have been provided by the ERD. We thus carry out a joint inversion of these teleseismic and strong-motion data using the method of Yoshida and Koketsu (1990) and Yoshida et al. (1996).

2. Data and method

Milkereit et al. (2000) observed surface ruptures along a 45-km segment of the western NAF, which extends bilaterally east and west from the epicenter. This rupture segment almost coincides with the full length of the Düzce fault segment of the NAF as shown in Fig. 2. Fig. 2 also shows aftershocks of the Izmit and Düzce earthquakes. Those that occurred after the Düzce earthquake are plotted with open circles, showing a distribution along a 60-km segment of the Düzce fault, whereas earlier aftershocks (of the Izmit earthquake) are plotted with solid circles. Given this distribution, we define a model fault plane for the Düzce earthquake with dimensions of 65×25 km, with strike 264° and dip 64°. We divide this model fault plane into 13×5 sub-faults with dimensions of 5×5 km.

To calculate the Green's function for each model seismic source, each sub-fault is approximated as a point dislocation located at its center. The source time function of this dislocation is expressed by superposition of several ramp functions with a common rise

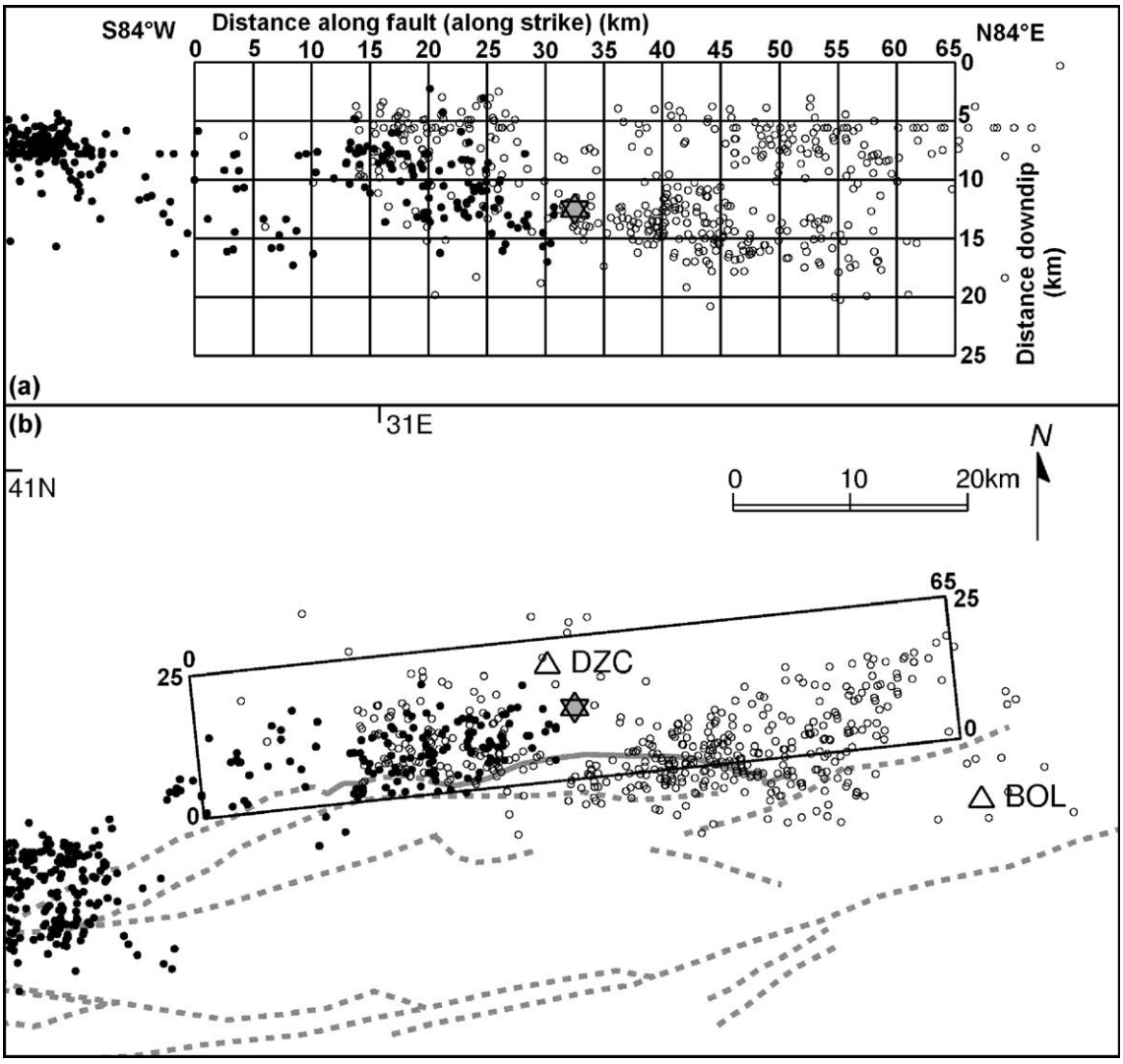

Fig. 2. Vertical cross-section (a) and map (b) illustrating the geometry of our model fault plane in relation to the aftershock zones of the Izmit (solid circles) and Düzce (open circles) earthquakes, respectively. In (a), these aftershocks have been projected onto the model fault plane. Solid gray line in (b) indicates the 45-km segment of surface faulting in the Düzce earthquake (from Milkereit et al., 2000). Dashed gray lines mark other faults within this part of the North Anatolian Fault Zone. Rectangle in (b) indicates the projection of the model fault plane onto the Earth's surface.

time, and the interval between adjacent functions is assumed equal to this rise time. Since the slip orientation of the Düzce earthquake has already been determined as right-lateral, but may not be purely right-lateral, and may include local variations, the slip vector **X** on each sub-fault is represented by a linear combination of two components with rake directions of $\pm 135^\circ$ (i.e., $\pm 45^\circ$ relative to a pure right-lateral rake of -180°). A slip vector with any rake between these limits can be expressed as a linear combination of such components, with weight factors A and B (where $B \equiv \sqrt{(1-A^2)}$, as the two vectors are perpendicular) as

$$\mathbf{X} = A \times [\text{the } -135^\circ \text{ vector}] + B \times [\text{the } +135^\circ \text{ vector}].$$

If A=B, the slip is purely right-lateral. However if B>A, the resultant rake is between 135° and 180°, and

thus slight reverse dip-slip is included. On the other hand, in our case $B<A$, so that slight normal dip-slip is included.

The time function is represented as

$$T = \mathbf{X}_1 T(t) + \mathbf{X}_2 T(t-\tau) + \mathbf{X}_3 T(t-2\tau),$$

where $\mathbf{X}_1$, $\mathbf{X}_2$, and $\mathbf{X}_3$ are vectors of the form of $\mathbf{X}$ calculated above. If $\mathbf{X}_1=\mathbf{X}_2=0$ in an inversion result, there is no slip in the windows t to $t+\tau$ and $t+\tau$ to $t+2\tau$. The slip is thus delayed by 2τ, where τ is the rise time. This modeling method can express variation in local rupture as well as variations in slip angles and source time functions (Yoshida et al., 1996).

We chose data from 14 teleseismic stations at epicentral distances between 30° and 90°, for which there is no complication in the P and S waves due to the Earth's structure. Station BDFB at an epicentral distance of 92° was also included to improve azimuthal coverage (Fig. 3). We retrieved long-period records from the IRIS-DMC, and numerically integrated their P-wave portions to obtain displacement waveforms with a sampling rate of 1.0 s. We calculated the ray-theoretical Green's functions for these teleseismic data using the PREM Earth model (Dziewonski and Anderson, 1981), assuming that these P-waveforms consist of direct P phases followed by surface-reflected pP and sP phases. An attenuation operator was applied with a time constant (t^*) of 1 s.

For the strong-motion data, we chose the four stations closest the epicenter of the Düzce earthquake (as shown in Fig. 1). We integrated the acceleration records provided by ERD to obtain velocity waveforms. The resultant velocities were filtered with a pass band of 0.05 to 0.5 Hz and then resampled with an interval of 0.5 s. We calculated the Green's functions for these strong-motion data using the reflectivity method developed by Kohketsu (1985). Since these records do not include accurate timing

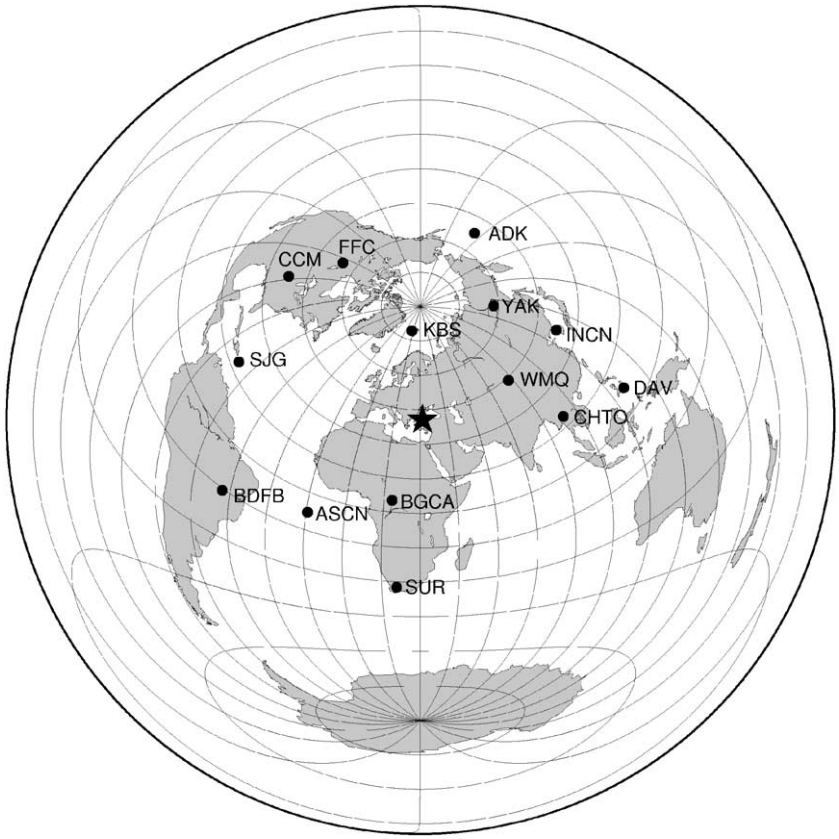

Fig. 3. Teleseismic stations used in this study. The star symbol represents the epicenter of the Düzce earthquake.

Table 1
Velocity structure

Notes	H (km)	V_p (km/s)	V_s (km/s)	ρ (g/cm^3)	Q_p	Q_s
1	0.40	1.40	0.70	2.00	100	50
2	1.00	2.20	1.10	2.20	200	100
3	7.00	4.00	2.00	2.40	300	150
3	5.00	6.00	3.40	2.70	500	250
3	6.00	6.60	3.70	2.90	800	400
3	7.00	7.20	4.00	3.05	800	400
3	∞	8.15	4.60	3.35	1000	500

This layered velocity structure was used in calculations of synthetic seismograms at the strong-motion stations. For each layer, H is the thickness, ρ is the density, and V_p, Q_p, V_s, and Q_s are the velocities and quality factors for anelastic attenuation, for P- and S-waves, respectively.

Notes:

(1) This layer was only included for station DZC.

(2) This layer was included for stations BOL, MDR and DZC.

(3) This layer was included for all four stations.

information, we make time corrections for observed P-wave arrivals by comparing the observed and synthetic seismograms. The layered velocity structure used for calculating synthetic seismograms at all four strong motion stations is illustrated in Table 1.

3. Results

We first carried out preliminary inversions of the teleseismic data to find an appropriate rupture velocity. The fault rupture was assumed to be initiated at the hypocenter determined by the SABO network (star in Fig. 2). We examined velocities in the range 1.5–3.0 km/s, and achieved the best match between the observed and synthetic waveforms with a value of 2.4 km/s. We then examined rise times of 0.5, 1.0 and 1.5 s, assuming the source time function to consist of three ramp functions, and found that 1.0 s gave a better fit than the others. We also examined a source time function consisting of five ramp functions, each with a rise time of 1.0 s, but found no significant improvement in the waveform matching. We therefore adopted the solution with the three ramp functions as our preferred solution from the inversion of the teleseismic data alone (Fig. 4).

The slip distribution in Fig. 4 reveals two asperities (patches of fault with the greatest slip) where slip in excess of 1.8 m was deduced, concentrated between depths of 5 and 15 km. Rupture was initiated at the hypocenter between them and propagated bilaterally through these asperities. The total seismic moment of this source model was 5.5×10^{19} N m, corresponding to M_w 7.1. Since the average rake angle in this source model was -172.2°, this slip distribution includes slight (normal) dip-slip components. The eastern asperity was clearly stronger than the western one, the moment release from the eastern half of the fault plane (3.3×10^{19} N m) was 1.5 times larger than that from its western half (2.2×10^{19} N m). The waveform match for this solution is satisfactory as shown in Fig. 5.

The strong-motion data were now jointly inverted with the teleseismic data in the final stage of this study. The assumptions about the fault model were kept the same as before. Considering the quality of the observed records, we determined their relative weights so that the signal-to-noise ratios of the teleseismic and strong-motion data are 10% and 20% of their maximum amplitudes, respectively. Fig. 6 shows the resultant slip distribution from this joint inversion. Two shallow asperities still exist in this slip distribution, but the western one has been weakened (seismic moment on the western half of the fault plane now 1.7×10^{19} N m). The largest slip, now 2.6 m, is recovered in the center of the eastern asperity, which is predicted to have released a similar moment to that in the previous inversion. The total moment is slightly reduced to 5.0×10^{19} N m, which again corresponds to M_w 7.1. The averaged rake angle of -171.8° is almost the same as before.

The eastern tip of the aftershock distribution of the Izmit earthquake (solid circles in Fig. 6) coincides with the point of rupture initiation, that is, the hypocenter, of the Düzce earthquake. The asperities (revealed by concentrations of aftershocks) extend from 5 to 15 km depth, similar to the teleseismic result. The aftershocks of the Düzce earthquake (open circles in Fig. 6) appear to be distributed along the upper and lower boundaries of this western asperity, whereas the earlier aftershocks of the Izmit earthquake occurred within this asperity.

Fig. 7 indicates that the joint inversion achieves an overall waveform match as good as for the inversion of the teleseismic data alone. The amplitude of the strong motion record at SKR, west of the epicenter, was several times smaller than that at BOL, to the

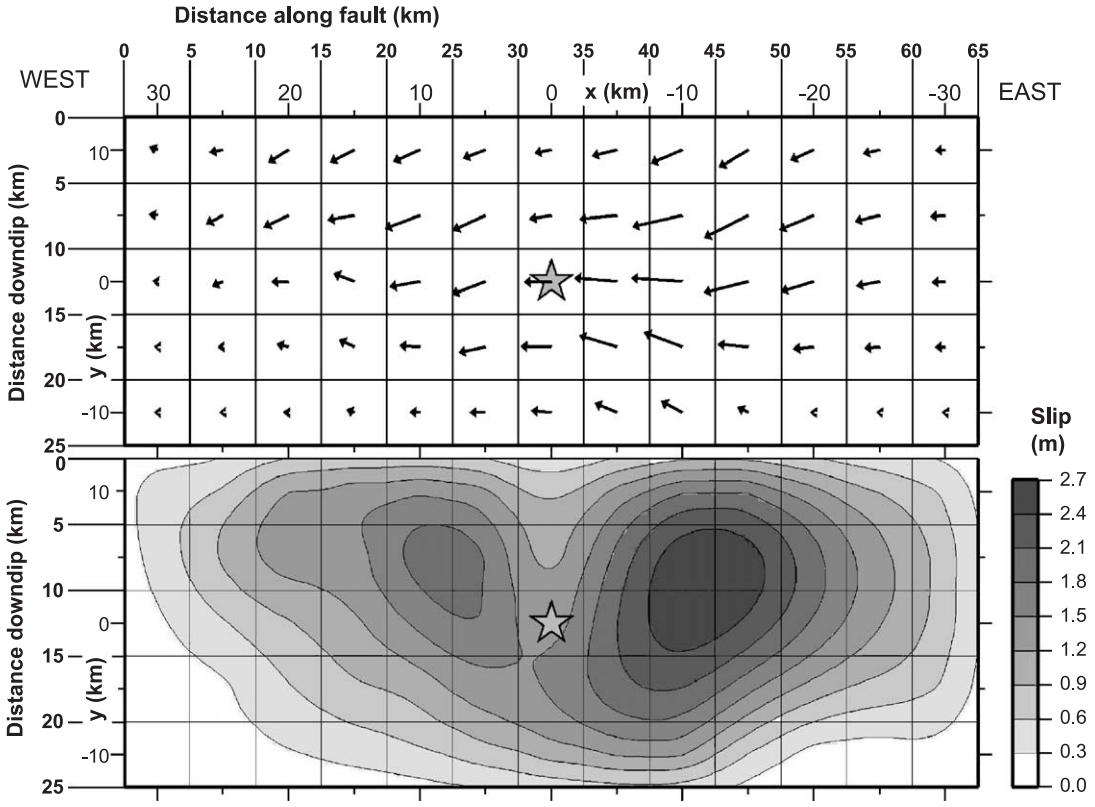

Fig. 4. Solution from the inversion of the teleseismic data alone. We show the slip vectors of the southern block relative to the northern block in the upper frame, and slip the distribution in the lower frame. Co-ordinates x and y indicate the positions of the grid of notional point seismic sources used. Rupture initiation is assumed to have occurred at (x=0 km, y=0 km) as indicated by the star symbol.

east. We predict that this difference results from the small moment release on the western half of the model fault plane, mentioned above. Our predicted asymmetric slip distribution and shallow depths of asperities agree with the observed surface rupture (Fig. 2; Milkereit et al., 2000) and the damage distribution (Kandilli Observatory, 1999).

4. Discussion and conclusions

The rupture process during the 1999 Düzce earthquake has been deduced from the joint inversion of teleseismic and strong-motion data. Two shallow asperities have been resolved on the fault plane (strike: 264°; dip: 64°) and the rupture has been deduced to have propagated bilaterally through them. The strong-motion data contribute to determining the relative weakness of the western asperity. The maximum slip of 2.6 m is predicted in the center of the eastern asperity. The total seismic moment M_0 was 5.0×10^{19} N m (M_w 7.1) and the average rake angle was $-172°$. We thus calculate the average stress drop $\Delta\sigma$ as 7 MPa, using the equation (Yagi and Kikuchi, 2000)

$$\Delta\sigma = 2.5 \times M_0/S^{3/2},$$

where S is the area of fault that slipped more than 0.6 m, estimated as 45×15 km. This value is smaller than 12 MPa, estimated for the Izmit earthquake (Yagi and Kikuchi, 2000), and falls between the typical stress drops of 3 and 10 MPa for inter-plate and intra-plate earthquakes.

Aftershocks of an earlier earthquake cannot trigger a large earthquake like the Düzce event, but the coincidence of the eastern tip of the Izmit aftershock distribution and the rupture initiation point of the

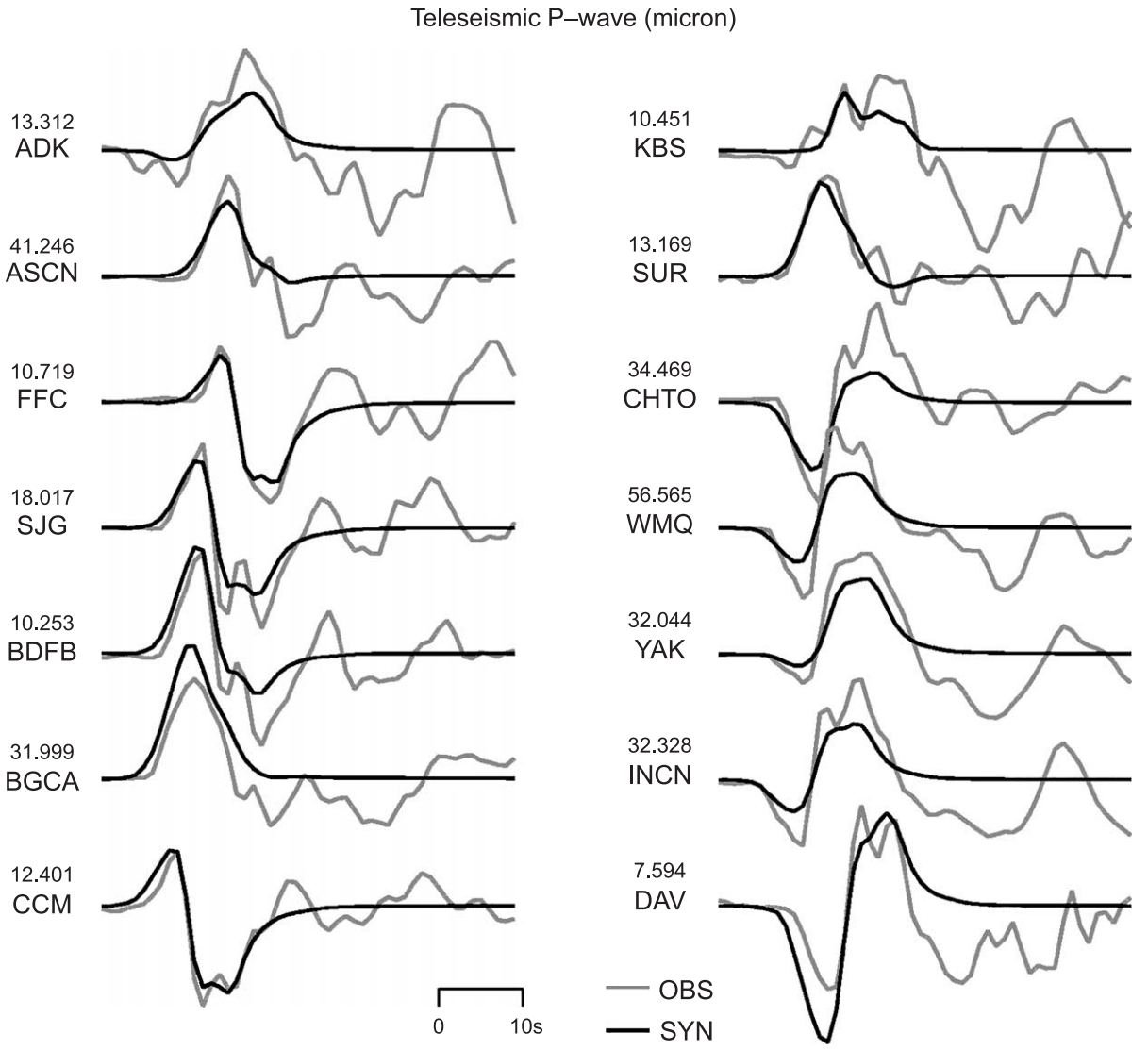

Fig. 5. Comparison of the observed (gray lines) and synthetic seismograms (black lines) for the solution from the inversion of the teleseismic data alone (Fig. 4). The maximum displacements are indicated in μm above the station codes.

Düzce earthquake may imply an indirect relation between the aftershocks of the Izmit earthquake and the triggering of the Düzce event. Iio et al. (2002) suggested that these aftershocks indicate afterslip following the Izmit earthquake, and this afterslip could concentrate stress in the source area of the Düzce earthquake. This stress concentration, in conjunction with the stress change due to the Izmit mainshock (e.g., Parsons et al., 2000), may have triggered the Düzce earthquake, since the aftershocks of the Izmit earthquake did not occur along the edges of the western asperity of the Düzce earthquake, but within this asperity.

Acknowledgements

We are grateful to Yuji Yagi and Helmut Grosser for their valuable suggestions and assistance. The careful review by editor Rob Westaway greatly improved the

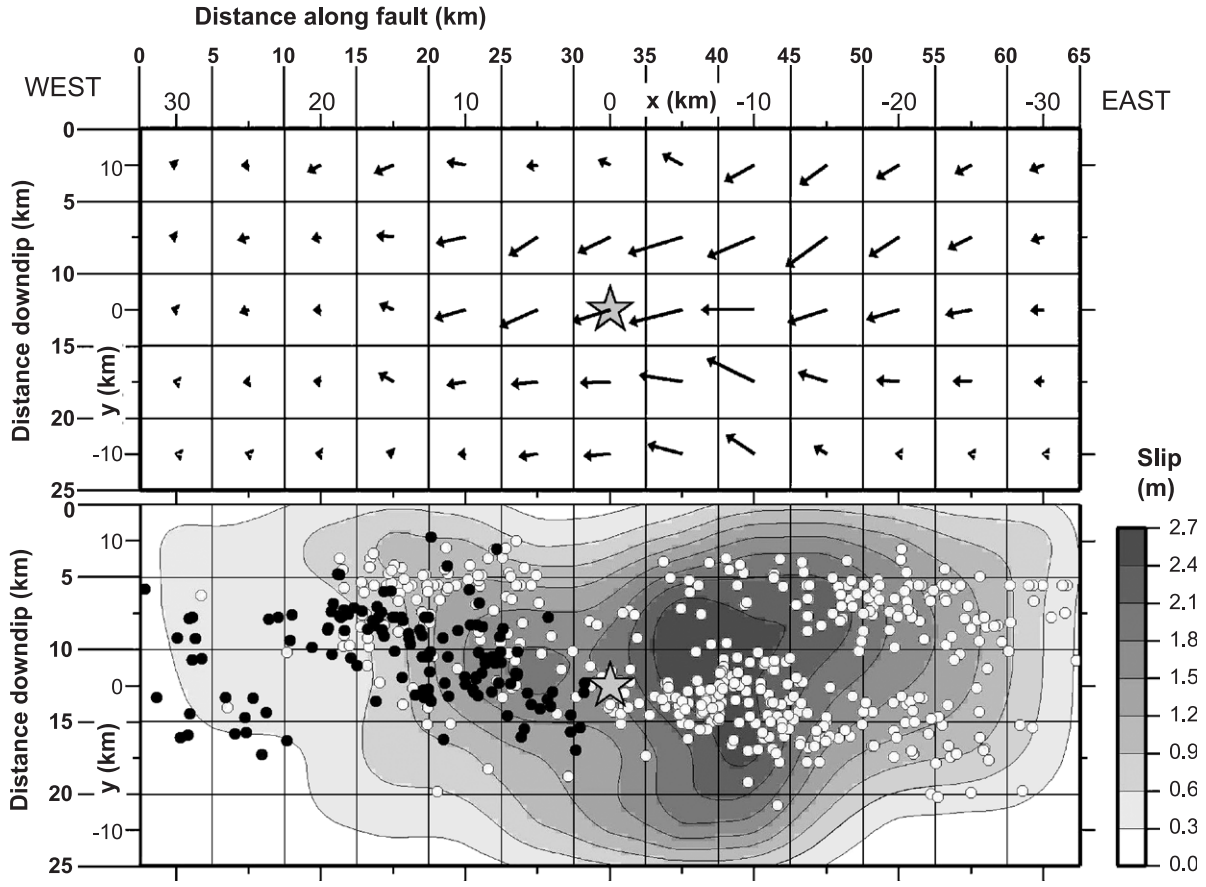

Fig. 6. Solution from the joint inversion of the teleseismic and strong-motion data. The aftershocks of the Izmit earthquake (solid circles) and Düzce earthquake (open circles) are plotted in the lower frame. The notation and geometry are otherwise as in Fig. 4.

manuscript. Comments by the anonymous reviewers were also very helpful. We thank Michael Baumbach, Helmut Grosser, Erwin Günther, Wolfgang Welle and Ünal Dikmen for observations of the surface rupture; Altan Necioðlu, Birger Lühr and Tuncay Taymaz for their support; and IRIS, GFZ and ERD for providing us with the waveform data. Figs. 1, 3, 4 and 6 were drawn using the GMT software (Wessel and Smith, 1991). This study was carried out while Nur Umutlu was a visitor at the International Institute of Seismology and Earthquake Engineering, Japan.

References

Akyüz, H.S., Hartleb, R., Barka, A., Altunel, E., Sunal, G., Meyer, B., Armijo, R., 2002. Surface rupture and slip distribution of the 12 November 1999 Düzce earthquake (*M* 7.1), North Anatolian Fault, Bolu-Turkey. Bull. Seismol. Soc. Am. 92, 61–66.

Ayhan, M.E., Bürgmann, R., McClusky, S., Lenk, O., Aktug, B., Herece, E., Reilinger, E., 2001. Kinematics of the Mw=7.2, 12 November 1999, Düzce, Turkey earthquake. Geophys. Res. Lett. 28, 367–370.

Dziewonski, A.M., Anderson, D.L., 1981. Preliminary reference Earth model. Phys. Earth Planet. Inter. 25, 297–356.

Iio, Y., Horiuchi, S., Baris, S., Celik, C., Kyomen, J., Ucer, B., Honkura, Y., Isikara, A.M., 2002. Aftershock distribution in the eastern part of the aftershock region of the 1999 Izmit, Turkey, earthquake. Bull. Seismol. Soc. Am. 92, 411–417.

Kandilli Observatory, 1999. http://www.koeri.boun.edu.tr//depremmuh/duzceq.htm.

Kiratzi, A., Louvari, E., 2001. Source parameters of the Izmit-Bolu 1999 (Turkey) earthquake sequences from teleseismic data. Ann. Geophys. 44, 33–47.

Kohketsu, K., 1985. The extended reflectivity method for synthetic near-field seismograms. J. Phys. Earth 33, 121–131.

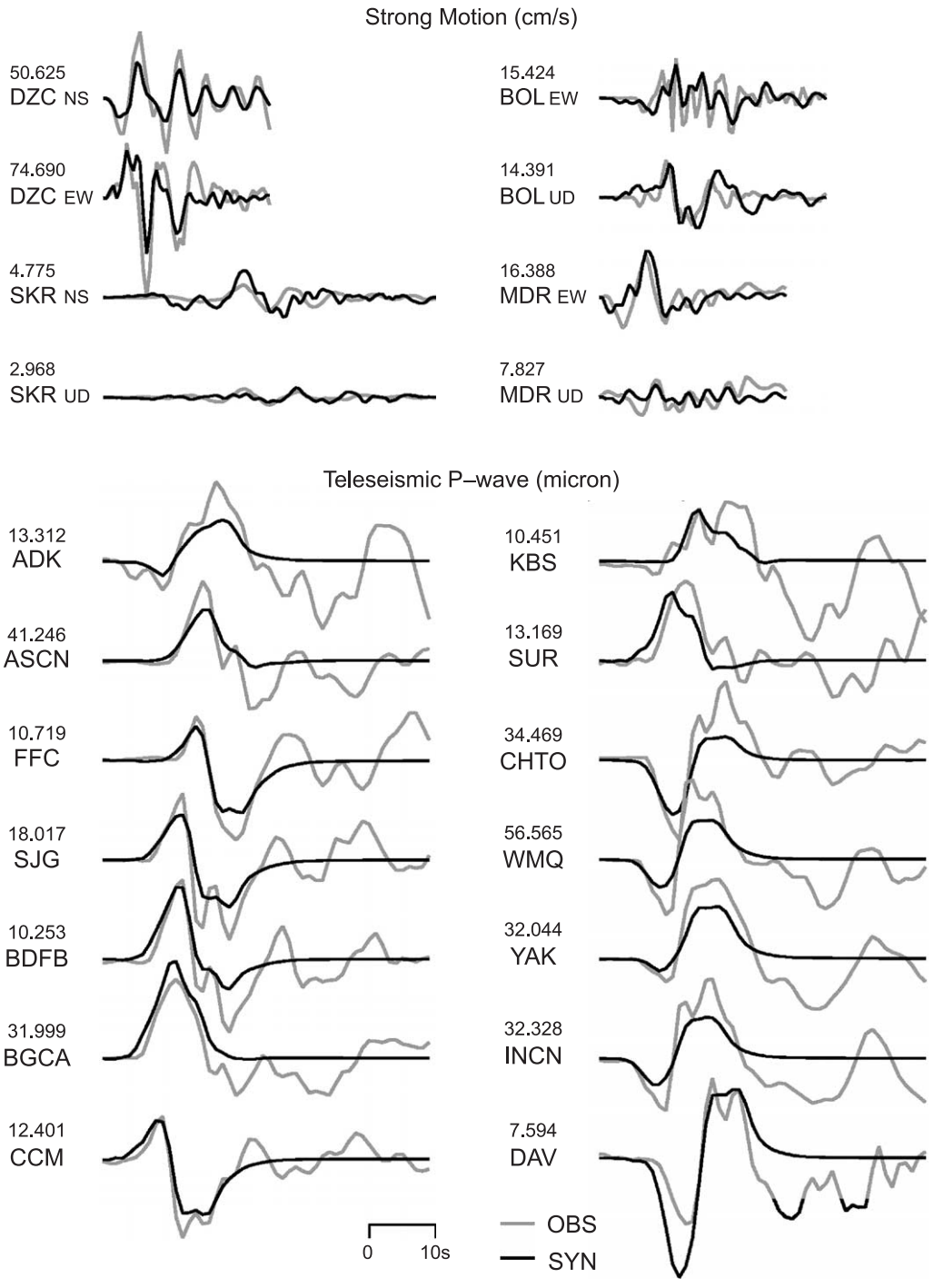

Fig. 7. Comparison of the observed (gray lines) and synthetic seismograms (black lines) for the solution from the joint inversion of the teleseismic and strong-motion data (Fig. 6). The maximum velocities (upper, in cm/s) and displacements (lower, in μm) are indicated above the station codes.

Milkereit, C., Zunbul, S., Karakisa, S., Iravul, Y., Zschau, J., Baumbach, M., Grosser, H., Gunther, E., Umutlu, N., Kuru, T., Erkul, E., Klinge, K., Ibs von Seht, M., Karahan, A., 2000. Preliminary aftershock analysis of the Mw=7.4 Izmit and Mw=7.1 Düzce earthquake in western Turkey. In: Barka, A., Kozaci, Ö., Akyüz, S. (Eds.), The 1999 Izmit and Düzce Earthquakes: Preliminary Results. Istanbul Technical University, ISBN: 975-561-182-7, pp. 179–187.

Nábêlek, J.L., 1984. Determination of earthquake source parameters from inversion of body waves. Ph.D. thesis, Massachusetts Institute of Technology, Cambridge, Massachusetts.

Parsons, T., Toda, S., Stein, R., Barka, A., Dieterich, J., 2000. Heightened odds of large earthquakes near Istanbul: an interaction-based probability calculation. Science 288, 661–665.

Tibi, R., Bock, G., Xia, Y., Baumbach, M., Grosser, H., Milkereit, C., Karakisa, S., Zunbul, S., Kind, R., Zschau, J., 2001. Rupture processes of the 1999 August 17 Izmit and November 12 Düzce (Turkey) earthquakes. Geophys. J. Int. 144, F1–F7.

Wessel, P., Smith, W.H.F., 1991. Free software helps map and display data. EOS, Trans., Am. Geophys. Union 72, 445–446.

Yagi, Y., Kikuchi, M., 2000. Source rupture process of the Kocaeli, Turkey, earthquake of August 17, 1999, obtained by joint inversion of near-field data and teleseismic data. Geophys. Res. Lett. 27, 1969–1972.

Yoshida, S., Koketsu, K., 1990. Simultaneous inversion of waveform and geodetic data for the rupture process of the 1984 Naganoken-Seibu, Japan, earthquake. Geophys. J. Int. 103, 355–362.

Yoshida, S., Koketsu, K., Shibazaki, B., Sagiya, T., Kato, T., Yoshida, Y., 1996. Joint inversion of near- and far-field waveforms and geodetic data for the rupture process of the 1995 Kobe earthquake. J. Phys. Earth 44, 437–454.